Drug Delivery and Translational Research (2019) 9:1143–1158
https://doi.org/10.1007/s13346-019-00660-z

ORIGINAL ARTICLE

Accelerated and scarless wound repair by a multicomponent hydrogel through simultaneous activation of multiple pathways

Dipsikha Bhattacharya[1,2] · Ratnakar Tiwari[1] · Tejasvi Bhatia[1,4] · Mahaveer Prasad Purohit[1,4] · Anu Pal[1] · Pankaj Jagdale[1] · Mohana Krishna Reddy Mudiam[1,4] · Bhushan Pradosh Chaudhari[1] · Yogeshwar Shukla[1,4] · Kausar Mahmood Ansari[1,4] · Ashok Kumar[5] · Pradeep Kumar[3] · Vikas Srivastava[1,4] · Kailash Chand Gupta[1,3,5]

Published online: 17 July 2019

Abstract

Scarless healing of injury remains a clinical challenge because of its complicated and overlapping phases of inflammation, clearing, and regeneration. Curcumin has been already established as a potential wound healing agent for normal and diabetic-impaired wounds. Herein, the question has been addressed whether a well-known antioxidant cerium oxide nanoparticle (CNP) can potentiate the activity of curcumin to promote a cellular program for scarless healing. In this study, we have developed a biocompatible poly (acrylamide) hydrogel (PAGE)-based dressing material comprising of CNP and curcumin (ACC) and tested its wound healing activity in an animal model of acute wound. Characterization of the CNP- and curcumin-entrapped hydrogel dressing (ACC) demonstrated high loading efficiency and sustained release of curcumin. In a full-thickness acute wound healing model of rat, a single application of ACC dressing demonstrated higher wound healing efficacy (78%) and negligible scarring compared to dressings containing only curcumin or CNP in 7 days. Enhanced cell proliferation, higher collagen content, advanced wound maturity, re-epithelialization, and granulation tissue formation were observed using the combination of curcumin and CNP (ACC). Study of cellular mechanisms identified MCP-1 and TGF-β as the key drivers of differential and accelerated healing observed in the ACC group. These, coupled with the upregulation of growth-related signaling pathways (HER2/ErbB2, TGF-β-Smad2/3, MAPK/ERK, AKT, and VEGF), promoted almost scarless healing in animals treated with ACC. The optimized combination of curcumin and CNP used in our study shows distinct advantage and can be a better agent for complete wound healing.

Keywords Cerium oxide nanoparticles · Curcumin · Wound healing · Anti-inflammatory · Antioxidant

Dipsikha Bhattacharya and Ratnakar Tiwari contributed equally to this work.

Electronic supplementary material The online version of this article (https://doi.org/10.1007/s13346-019-00660-z) contains supplementary material, which is available to authorized users.

✉ Vikas Srivastava
76.vikas@gmail.com

✉ Kailash Chand Gupta
kcgupta@igib.res.in

[1] CSIR-Indian Institute of Toxicology Research (CSIR-IITR), Vishvigyan Bhavan, 31 Mahatma Gandhi Marg, P.O. Box No. 80, Lucknow, Uttar Pradesh 226 001, India

[2] Department of Chemistry, School of Science, Adamas University, Jagganthpur, Kolkata, West Bengal 700126, India

[3] CSIR-Institute of Genomics and Integrative Biology, Delhi University Campus, Mall Road, Delhi 110007, India

[4] Academy of Scientific and Innovative Research (AcSIR), CSIR-IITR Campus, Lucknow, India

[5] Department of Biological Sciences and Bioengineering (BSBE) and Centre for Environmental Science and Engineering (CESE), Indian Institute of Technology, Kalyanpur, Kanpur, Uttar Pradesh 208016, India

Background

Impaired healing of skin wounds and further medical complications may result in permanent damage and even mortality [1]. This increases the importance of wound management to our healthcare systems. Wound repair is a highly complicated and coordinated process that involves several interrelated but dynamic stages. The initial inflammatory phase involves recruitment of phagocytic cells and clearing of wounds while the proliferative phase controls cell migration, granulation, contraction, and re-epithelialization. Finally, the matrix remodeling phase involves connective tissue formation and strengthening of newly formed epithelium [2, 3]. A delicate balance between factors promoting inflammation, cell migration, and repair is essential for scarless healing. However, this process is often disrupted in severe pathological conditions leading to chronic inflammation, oxidative stress, and impaired healing [4, 5]. Therefore, the ultimate goal of a wound healing agent is to promote speedy recovery with minimal scarring and maximal restoration of function. Though many wound dressing materials such as chitosan, cerium oxide, gold, or nanocurcumin modified scaffolds are reported by several groups [1, 3–6], there is still a pressing need for an improved one which could promote healing with minimum scarring.

The wounds may be classified as acute or chronic depending on their progression and the time taken to heal. At the onset, most new wounds are acute. Depending on the body response and the process of healing and the factors involved, the wound may heal completely or progress to a chronic state with uncontrolled inflammation and excess deposition of extracellular matrix components causing permanent scarring. The goal of an ideal wound healing agent is to drive a repair program which limits inflammation and promotes scarless healing.

An ideal healing material should be composed of bioactive substances which help in maintaining a moist environment, protect microbial infection, provide thermal insulation, permit gaseous exchanges, quench reactive oxygen species (ROS), and control inflammation [6–8]. Being identified as a natural healing agent, curcumin was found to possess a wide range of beneficial pharmacological properties including anti-inflammatory, anti-oxidant, anti-microbial, and anti-cancer activities [9]. Several in vitro and in vivo studies have demonstrated curcumin as a promising anti-inflammatory and antibiotic agent both in normal and diabetic-impaired wounds [10–13]. Curcumin promotes wound healing by increasing the granulation tissue and enhancing the biosynthesis of transforming growth factor (TGF-β) as well as inhibiting pro-inflammatory cytokines (interleukin-1, interleukin-8, and tumor necrosis factor) [6, 14]. The antioxidant property of curcumin is also shown by its ability to protect fibroblast and keratinocytes against peroxide-induced oxidative stress [4, 15]. Although many innovative curcumin nanoformulations have been reported with the enhanced water solubility and bioavailability using various polymers, its extremely poor water solubility and degradation in alkaline medium still raise the need of developing novel nanoscale scaffolds with improved therapeutic purposes [4, 16–18].

In recent years, CNP (nanoceria) has shown great potential as biocompatible antioxidant and anti-inflammatory nanoagents as they can mimic the catalytic activities of superoxide dismutase, peroxidase, and catalase [19]. This unique property of CNP is governed by the reversible switch of its oxidation state, with the regenerative capacity of Ce^{3+} [20]. Therefore, CNP have been used as potential therapeutics in numerous biological systems such as in biosensing [21], biomedicine [22], drug delivery [23], and bio-scaffolding [24] applications. This unique regenerative ability of CNP was generated due to its neuro-protective [14, 25], radioprotective [26], and anti-inflammatory [27] properties. Recently, CNP has also been found as a powerful wound healing agent in both in vitro and in vivo model [1, 28].

As a promising dressing material, hydrogels are preferred because they provide a moist and hydrated environment ideal for complete repairing process [29, 30]. Furthermore, they mimic the key attributes of porous and tissue-like consistency, and their functionalized network can control the delivery as well as release of bioactive substances to the wound [3, 29–33]. Several wound healing studies reported polyelectrolyte gel such as polyacrylamide (PAGE) hydrogel as an ideal healing scaffold as their internal interactions with the bioactive drug can enhance the drug release, thereby increasing its efficacy [34]. Recently, 2-acrylamido-2-methylpropanesulfonic acid sodium salt (AMPS) has received emerging attention as an anionic monomer in fabricating polyelectrolyte gel-based dressing due to their strongly ionizable sulfonate ($–SO_3H$) groups [35, 36] and capability of anchoring cationic ions [37] as well as reduced protein adsorption or platelet adhesion ability [38]. Therefore, AMPS has played a key role towards fabricating metal nanoparticle-entrapped polyelectrolyte hydrogels with improved mechanical properties and controlled biological activities. It was already reported that the charged backbone of AMPS-based polyelectrolyte gel easily facilitates the immobilization as well as formation of metallic nanoparticles, thereby promoting the formation of new metal nanoparticle-entrapped polyelectrolyte gel with enhanced antibacterial as well as wound healing ability [39–41].

In this study, we have optimized the combination of CNP and curcumin and developed it into a wound healing hydrogel scaffold (ACC) to promote a balanced microenvironment in the wounded tissue. The large surface area of the polyelectrolyte hydrogel could provide an ideal environment for wound hydration and promote sustained delivery of CNP and curcumin to limit inflammation and promote epidermal cell proliferation and wound re-epithelialization.

We have evaluated the therapeutic efficacy of the developed formulations in an acute wound healing model and also

identified key cell signaling mechanism involved in accelerating wound healing using our formulation.

Experimental section

Materials

All chemicals and reagents used in this study were of analytical grade, unless otherwise stated. Curcumin, cerium nitrate hexahydrate [$Ce(NO_3)_3.6H_2O$], acrylamide (AA), acrylamido-2-methylpropane sulfonic acid (AMPS), N, N′-methylene bisacrylamide (MBA), N, N′, N″, N″'-tetramethylethylenediamine (TEMED), ammonium persulfate (APS) were procured from Sigma-Aldrich (St. Louis, MO, USA). Acetone and ethanol were purchased from Merck, (Darmstadt, Germany). All the solvents used in this study were procured from S. D. Fine Chemicals Pvt. Ltd. limited (Mumbai, India) and Merck (Darmstadt, Germany). All reagents used in this article were of analytic reagent (AR) grade, and used as received.

Preparation of desired curcumin and CNP-loaded AA-AMPS hydrogels

Four different hydrogels were synthesized and evaluated in an ex vivo wound healing animal model, and they are curcumin-loaded CNP entrapped poly (acrylamide) (AA-AMPS) hydrogel [ACC], curcumin-loaded poly (acrylamide) AMPS (AA-AMPS) hydrogel [AC'], CNP-loaded poly (acrylamide) AMPS (AA-AMPS) hydrogel [AC], and void poly (acrylamide) AMPS (AA-AMPS) hydrogel [A]. To avoid confusion, poly (acrylamide) AMPS (AA-AMPS) hydrogel was shown as void A hydrogel and the other three hydrogels were abbreviated as ACC, AC', and AC gels accordingly. For the synthesis of the desired ACC, three consecutive steps were involved as displayed in Fig. S1. These steps include synthesis of Ce^{3+} ion-loaded A hydrogel, CNP-loaded A hydrogel (abbreviated as AC which was also used as a control in this study), and finally, the curcumin-entrapped CeO_2-A hydrogel (abbreviated as ACC), the desired material for ex vivo wound healing. Curcumin-entrapped A hydrogel (abbreviated as AC') and void A hydrogel (abbreviated as A) are also fabricated without Ce^{3+} loading to study their effects as controls of ACC and AC on ex vivo rat skin healing. The synthesis of A, ACC, AC, and AC' and A gels were described accordingly in the following section.

Synthesis of void A hydrogel

Firstly, A hydrogel was prepared by solution polymerization in a 100-ml round bottom flask following the procedure reported earlier with minor modifications [41]. Acrylamide (10.968 g, 25.74 mM) and AMPS (2.67 ml, 2.5 mM, ratio of AA:AMPS ~ 10:1) were dissolved in 24 ml of millipure water under N_2 atmosphere for 30 min at ambient temperature (25 °C). The amounts of all the chemicals used were six times of their mole ratios in order to prepare five sets of void gel plates to apply on all animals of each time points (30 rats of each time points). To this, 60 ml of MBA, known as the cross-linking agent (50 mg/10 ml, ratio of AA:MBA ~ 80:1), was added and kept at 0 °C for another 30 min to initiate accurate mixing. The free radical polymerization was carried out after the instant addition of 6 ml of APS (300 mg, 1.3 mM) and TEMED (78 μl, 0.5 mM) as redox-initiating pair. After 4 h of concomitant stirring, 20 ml of the solution was poured in each of the five sets of tissue culture dishes (60 mm) and kept at 37 °C for complete gelation. After the formation of the required gel, it was repeatedly washed with distilled water for three times, frozen overnight at − 20 °C and then lyophilized at − 110 °C for overnight in a freeze dryer. In this way, void AA:AMPS (A) hydrogel scaffolds with different ratios of AA:MBA (20:1, 40:1, and 80:1) were prepared, and the final ratio of AA:MBA was optimized (keeping the ratio of AA and AMPS contents constant).

Synthesis of CNP-entrapped A hydrogel (AC)

For the synthesis of AC gel, $Ce(NO_3)_3{\cdot}6H_2O$ (521 mg, 0.2 mM) was added in the reaction mixture containing acrylamide, AMPS, and MBA (best composition) in the same ratio as required to prepare void A gel, and the same polymerization procedure entrapping Ce^{3+} ions was repeated for the synthesis of AC gel. After 4 h of concomitant stirring, these solutions were poured in six tissue culture petri plates (60 mm), kept at 37 °C, repeatedly washed with distilled water for three times, frozen overnight at − 20 °C, and then lyophilized at − 110 °C for overnight in a freeze dryer. After that, the required CNP-loaded A gel or AC gel was fabricated by gently oxidizing each set of Ce^{3+} cross-linked gel using 20 ml of 1% H_2O_2 for 4 h at 25 °C. The formation of CNP, i.e., CeO_2 NPs inside the gel matrix was clearly indicated by the instantaneous change of color from white to light yellow signifying the formation of CNP inside the gel matrix. This gel was finally washed with distilled water repeatedly, frozen, and then lyophilized in a freeze dryer as described above. Two more AC hydrogels were prepared using 0.1 and 0.4 mM of Ce^{3+} ions, and best composition was chosen from further characterizations.

Synthesis of curcumin-entrapped CNP-loaded hydrogel (ACC)

The curcumin-entrapped CNP-loaded AC hydrogel (ACC) was fabricated using the previously described synthetic procedure of AC gel fabrication followed by the successful loading of curcumin. Briefly, after the fabrication of AC gel, 20 ml of curcumin (100 mg/20 ml in acetone: water) [42] was mixed

in each set of the five plates of AC gels as previously described and kept for 48 h at 25 °C in dark condition. The hydrogel and drug ratio was maintained in the ratio of 20:1. These five plates containing curcumin solution for complete entrapment were washed repeatedly with distilled water, frozen, and lyophilized as described above for void A and AC gels respectively.

Synthesis of curcumin-loaded void A hydrogel (AC')

For the synthesis of AC' hydrogel, the same ratio was maintained for all the other chemicals and the same procedure was repeated for the synthesis as followed for ACC gel without Ce^{3+} imprinting. After 4 h of concomitant stirring, these solutions were poured in six tissue culture Petri plates (60 mm), kept at 37 °C, and were repeatedly washed with distilled water for three times. These gels were lyophilized at − 110 °C for overnight maintaining the same condition as used for A gel. Then, to prepare AC' hydrogel, curcumin was loaded inside these A gels maintaining the same hydrogel to drug ratio (20:1) of as used for ACC gels and kept for 48 h at 25 °C in dark condition. These five plates containing curcumin solution for complete entrapment were washed with distilled water repeatedly, frozen overnight at − 20 °C, and then lyophilized in a freeze dryer.

Swelling ability of gels

For the swelling ability study, dried A hydrogels (prepared by using different A:MBA ratios) were cut into small pieces that had equal weights (500 mg) and were immersed in phosphate-buffered saline (PBS) (pH 7.4, 37 °C). After each time interval, the hydrogels were taken out, soaked with filter paper, and were immediately weighed (W_w). Each experiment was repeated 3 times, and the average value was taken as the percentage water adsorption.

$$\mathrm{DS} = \frac{(W_W - W_d) \times 100}{W_d} \tag{1}$$

Here, DS is the percentage/degree of swelling and W_w and W_d represent the wet and dry weight of the A scaffolds at equilibrium, respectively.

Tensile testing ability of hydrogels

The hydrogel specimens including all three A compositions and the AC gel (fabricated using AA: MBA 80:1) had designed the width of 10 mm and the thickness of 1 mm. The distance between the two clamps was 3 mm. During measurement, the membrane was pulled by the top clamp at a rate of 40 mm/min through a distance of 10 cm before the clamp was returned to its starting point [43]. The force and elongation before the membrane was broken were recorded. The tensile strength and elongation at breakage were calculated as follows.

$$\text{Tensile strength (MPa)} = \text{breaking force (N)} / \text{cross-sectional area of sample } (\text{mm}^2) \tag{2}$$

$$\text{Elongation at breakage (\%)} = \text{increase in length at breaking point (mm)} / \text{original length (mm)} \times 100 \tag{3}$$

Curcumin loading and entrapment efficiency

The amount of curcumin loading and the entrapment efficiency were determined by analyzing the ACC scaffold using Specord 210 Plus analytic jena, Optiplex 330 (Perkin Elmer) UV-Vis spectrophotometer (Germany). An almost circular ACC hydrogel (10 mm round and 500 mg in weight) was fabricated by accurately shaping the ACC mold using scissors and mentioned as ACC scaffold. It was degraded for 48 h in 10 ml of acetone: water mixture (1:1) under gentle shaking and the absorbance of the solution was measured at 428 nm [42]. The amount of curcumin entrapped inside this matrix was determined using a previously drawn calibration curve of curcumin using different concentrations. The percent drug loading (DL) and entrapment efficiency (EE) of ACC scaffold were calculated according to Eqs. (2) and (3). All the measurements were performed in triplicate. The same procedure was followed for the calculation of the DL and EE of AC' scaffold in order to compare the efficiency of ACC and AC' gels.

$$DL = \frac{Curcumin\,(Drug) \times 100\%}{Hydrogel + Curcumin\,(Drug)} \tag{4}$$

$$EE = \frac{Amount\ of\ actual\ Curcumin\ entrapped\ in\ Hydrogel \times 100}{Amount\ of\ Total\ Curcumin\ taken\ for\ entrapment} \tag{5}$$

Characterization of synthesized scaffolds (A, AC, ACC, and AC')

Fourier transform infrared (FTIR) spectra were recorded on a Thermo Scientific ID_5 ATR. The UV-Vis spectra were recorded on a Specord 210 Plus analytic jena, Optiplex 330 (Perkin Elmer) UV-Vis spectrophotometer (Germany). The phase analysis of the fabricated AC gel was performed on an X'pert Pro Phillips X-ray diffractometer with Cu Kα radiation. The mechanical properties of nanohydrogel scaffolds were evaluated using a Lloyd tensiometer (AMETEK, USA). The tensiometer was equipped with a 100 N load cell, in a manner consistent with the ASTM D638 standard. The

morphological variations were observed by using a scanning electron microscope (SEM) QUANTA™ FEG450, FEI (Eindhoven, The Netherlands). For this study, AC hydrogel scaffolds (each scaffold weighed 500 mg, these hydrogels were now renamed as scaffolds to give better impact of a wound patch in healing experiment compared to hydrogel) were with different cerium ion concentrations (0.1 mM, 0.2 mM, and 0.4 mM). They were cut into pieces and dispersed (hydrogels could not get dissolved in water) at a concentration of 10 mg/ml and drop casted on a thin glass slide coated with a thin layer of palladium gold alloy just before image under SEM. For TEM analysis, a drop of ACC gel dispersion (at a concentration of 1 mg/ml) was placed on a form over coated copper grid and air dried at 25 ± 2 °C. TEM analysis was also performed with AC' gel to ensure the size as well as morphology of the AC' gel without CNP loading. The morphology and size of these nanogels (ACC and AC') were visualized under the transmission electron microscope (FEI Company, OR, USA) operated at 80 kV, attached to a Gatan Digital Micrograph (PA, USA).

In vitro curcumin release from ACC scaffold

A modified dialysis method was employed to determine the in vitro release behavior of curcumin from ACC scaffold. Briefly, an accurately weighed scaffold (500 mg in dried condition) was placed in a dialysis bag (molecular cut off is 3.2 kDa). The bags were suspended in 50 ml of phosphate-buffered saline (PBS contain 50%, *v*/*v* of ethanol, pre-warmed to 37 °C), adjusted to pH 7.4 and shaken at 200 rpm for 5 days. At selected time intervals, 1 ml of sample was collected and replaced by an equal volume of fresh medium. The released drugs were quantified using both spectrophotometric analysis and ultra-performance liquid chromatography (UPLC). Determination of concentration of curcumin was carried out by Shimadzu Nexara UPLC equipped with quaternary pump liquid chromatography (LC-30AD), column oven (SPD-M20A), autosampler (SIL-30AC), degassing unit (DGU-20ASR), and prominence diode array detector (SPD-M20A). Chromatographic separations were performed on a reversed phase C-18 column (Synchronis, 100 mm × 2.1 mm × 1.7 μm). Column oven was maintained at 40 °C during analysis. Mobile phase (acetonitrile: 5% acetic acid, 75: 25, *v*/*v*) was used as an eluent at the flow rate of 1 mL/min for the separation of metabolites. All results were the mean of three samples, and all data were expressed as the mean ± SD. The same drug release and quantification procedures were followed for AC' gel, and the data is represented in Fig. S9.

Biocompatibility study of fabricated scaffolds

HaCaT cells (human keratinocytes from skin origin) [6] were cultured in Dulbecco's modified Eagle medium (GIBCO, Life Technologies) supplemented with 10% fetal bovine serum, 100 μg/mL penicillin, and 100 μg/mL streptomycin (pH 7.4). Keratinocyte cells were grown on 75-cm^3 cell culture flasks (Nunc) in a humidified atmosphere of 5% CO_2/95% air (*v*/*v*) at 37 °C. Cultures were passaged on reaching 80% confluence, using 0.05% trypsin-EDTA (GIBCO, Invitrogen, Carlsbad, California), and the medium was changed every 2 days. The experiments were performed at passage 5–6 for cell proliferation assays. Cell viability of the prepared scaffolds (void A, AC, AC', and ACC gels) was evaluated using the MTT assay for 24 h. For the assay, cells were plated overnight at a concentration of 10^4 cells/well in 96-well plates. Cells were exposed with five different concentrations of gel scaffolds (concentrations 100 μg/ml to 500 μg/ml), and viability was assayed by measuring optical density at 570 nm with 620 nm set as the reference wavelength using a microplate spectrophotometer (Biotek Power Wave XS, USA).

Full-thickness wounds and wound measurement

For the wound healing experiment, Wistar male rats (150 g, 7–8 weeks old) were obtained from the experimental animal facility of CSIR-Indian Institute of Toxicology Research (CSIR-IITR) and kept on a standard laboratory diet and water ad libitum. All the experiments were carried out with the permission of the Institutional Animal Ethics Committee of CSIR-IITR, India. In brief, animals were divided into five groups, each group comprising 6 rats: group I, commercial wound dressing (Medicare sterilized adsorbent cotton) was used as control (B); group II was (A); group III (AC); group IV (AC'); and group V (ACC). All the animals were anesthetized with ketamine hydrochloride and xylazine solution (9:1) by intra-peritoneal injection (30 mg/kg), and the dorsal area was shaved and disinfected using a depilatory cream. A full-thickness round excision wounds of approximately 10 mm (circular in shape) in diameter was then made on the back of the rats using surgical scissors and scalpels. For wound treatment, almost circular A, AC, ACC, and AC' hydrogel scaffolds of each 10-mm round and 500 mg weight were fabricated from lyophilized scaffolds (A, AC, ACC, and AC') using a scissor [16, 18, 43]. Then, each wound was covered fully using these circular scaffolds followed by final dressing with the transparent paraffin gauze dressing (Medicare B.P) as well as sterile adhesive bandage (Medicare) to prevent the rats from removing the treatments. Each rat was kept in a single cage for observation.

For wound healing studies, rats from each treatment group (five groups containing 6 animals) were observed for 0, 7, 3, and 14 days following wounding. For evaluation, all the sutures and occlusive dressings were removed, wounds were digitally photographed, and changes in the wound area were measured on days 7 and 14 using digital slide calipers. Wound

closure at each time points was calculated according to the equation:

$$\%\text{Wound closure or healing} = (A_o - A_t)/A_o \times 100 \quad (6)$$

where A_o is the initial wound area at the time of surgery of each rat and A_t is the open area of wound at the time of biopsy on days 0, 7, and, 14. Wound closure was the combined results of wound contraction and re-epithelialization. At day 3, no significant difference in healing (data not shown) was observed; therefore, the data for 7th and 14th days were represented. At each time point (0, 3, 7, and 14 days), animals were sacrificed under anesthesia and wounds were removed with surrounding tissues for analysis of pathological damage, granulation tissue formation, wound collagen content (Masson's trichrome staining), presence of growth and angiogenic factors, pro- and anti-inflammatory cytokines, antioxidant activity, and cell signaling pathways activated during healing.

Histopathology

Biopsy specimens including the central part of the wounds were fixed in formalin for 72 h. After fixation, tissues were sliced/trimmed and then processed for dehydration and wax impregnation using automatic tissue processor (MICROM), dehydrated through a graded ethanol concentration series, and cleared in xylene. Then, using Leica 2125, microtome tissue blocks were trimmed. Wound tissues were then sequentially sectioned at 5 μm using a microtome (Leica) and subsequently stained with hematoxylin and eosin (H&E) to assess the stages of healing and with Masson's trichrome (MT) blue staining (Sigma-Aldrich, USA) to study the extent of collagen deposition in healed tissue. Images were taken using a Leica camera (model DFC 295) on a Leica Microscope. For the H&E analysis, at least three wounds of three rats per time point were considered and images presented are representative of all the replicates. For MT staining, the same procedure was followed as H&E analysis [14, 18].

Cytokine profiling

For the evaluation of cytokine expression levels in wound healing, we used the bead-based multiplexing kit on a Luminex Magpix Platform (Austin, TX, USA). For cytokine level evaluation, blood samples from different groups (A, AC, AC', ACC, and B) were allowed to clot for 1 h at room temperature before centrifugation for 10 min at approximately 1500 rpm at 4 °C. The prepared serum was freshly stored in a refrigerator at − 80 °C before testing. For bead-based multiplex assay based on the principle of sandwich ELISA, 50 μl serum samples were incubated with antibody conjugated beads for 2 h at room temp. The beads were then washed using a magnetic separator and incubated with biotin-conjugated detection antibody for 30 min. This was followed by washing and addition of streptavidin-PE. The beads were then run on the Magpix system for quantification of the bound proteins. The results are expressed as pg/ml protein after plotting on a standard curve.

Multiplex analysis of total and phosphoproteins involved in cell signaling

For measuring different cell signaling intermediates, we used antibody-conjugated beads on a multiplex assay platform (Luminex Magpix, Austin, TX, USA). The assay is based on the principle of sandwich ELISA using two primary antibodies for different epitopes of an antigen. Assays were done for various total as well as phosphoproteins involved in cell signaling. Equal amounts of tissue lysate obtained from wound area were used for the assay after quantification of total protein concentration. Assays were done for Erk1/2, GSK3-β, HER2, IκB-α, JNK, MEK1, p38 MAPK, p70s6 kinase, and Smad2 total proteins. Assays were also done for the following phosphoproteins: Smad2 (Ser465/467), Akt (Ser473), GSK3 α/β (Ser21/Ser9), Erk1/2 (Thr102/Tyr204/Thr185/Thr187), JNK (Thr183/Tyr185), NF-κBp65 (Ser536), PDGFR-β (Tyr751), and STAT1 (Tyr701). The results are expressed as net median fluorescence intensity (MFI).

Statistical analysis

All data were recorded as the mean ± the standard deviation (SD). Statistical analysis between the multiple tested groups and control group was analyzed using one-way ANOVA with the Tukey's multiple comparison test (Graph Pad Prism 5.0). Values of $^{*}p < 0.05$, $^{**}p < 0.01$, and $^{***}p < 0.001$ (ANOVA with Tukey's multiple comparison test) were indicative of statistically significant differences. All experiments were performed at least three times.

Results and discussions

Fabrication and characterizations of the A, AC, AC', and ACC gel scaffolds

The goal for successful wound repair is accelerated healing without scars. A combination of agents which act on different aspects of wound repairing process will thus be useful. In this study, we have, therefore, introduced a unique hydrogel formulation by combining two well-known healing agents (curcumin and CNP) in an optimum ratio in a biocompatible hydrogel matrix. Acrylamide (AA) was chosen as our basic monomer because of its extensive use in the fabrication of polyacrylamide (PAGE) hydrogels that have been used in the field of tissue engineering [44]. AMPS were chosen due

to its pH-independent gelling behavior and capability of anchoring cationic ions as well as molecules. The scaffolds namely ACC, AC, AC', and A scaffolds were prepared through free radical polymerization between the monomer acrylamide (AA), comonomer (AMPS), and cross-linker (MBA) in the presence of Ce^{3+} and $–SO_3H$ ions using TEMED and APS at ambient temperature under N_2 atmosphere (Fig. S1). The synthesized AMPS-PAGE (A) hydrogels with different AA:MBA ratios (20:1, 40:1, and 80:1) were evaluated by their swelling ratio analysis (Fig. S2), and from this data, the fabricated gel using AA:MBA ratio of 80:1 and AA:AMPS ratio of 10:1 was chosen as our desired void hydrogel as it exhibited the highest swelling ratio. The mechanical properties of the various A hydrogels with different AA:MBA ratios were also measured and compared with composite AC gels. It is shown in Fig. S3 that A hydrogel with the best swelling result (80:1) had shown almost comparable tensile strength to composition (40:1) [43]. The structural morphology of these void hydrogels (A) was also analyzed by SEM studies, and it can be shown that A scaffold with the highest AA:MBA ratio exhibited relatively smoother surfaces compared to other compositions with porous morphology (Fig. S3). This gel (A) was combined with the CNP (antioxidant as well as anti-inflammatory) and curcumin (antioxidant, anti-infective, and wound healing) to fabricate a novel topical scaffold (ACC) for enhanced wound healing efficacy. The desired AC gel was made via optimizing the synthesis of AC hydrogels using three different concentrations (0.1 mM, 0.2 mM, and 0.4 mM) of cerium nitrate [$Ce(NO_3)_3$]. The formation of CNP inside the gel matrix (CNP-loaded A gel, i.e., AC gel) was confirmed from X-ray diffraction (XRD) analysis. From the XRD data (Fig. S4), the confirmatory crystalline fluorite like peaks of CNP along with the broad diffraction peak of poly (acrylamide) was visible, authenticating the successful formation of cubic CNP inside AC gel.

The formation of CNP within the gel network was verified by morphological analysis using SEM imaging (Fig. 1a–i). The morphology of fabricated AC gels displayed organized nanoflower-like gel structures which are completely different from void A gels which are mostly shapeless in nature. Each nanoflower (Fig. 1e) for 0.2 mM CNP-entrapped A gel] is likely to be made of many tiny nanopetals, which were spokewise oriented from a common central zone with surface defect, i.e., the active site on a roughened glass surface. Moreover, the most uniform AC nanogel (synthesized from 0.2 mM CNP) was comprised of highly distributed porous structures with interconnected nanopetal-like layers (shown in Fig. S5) compared to the other two compositions. Along with the uniform morphology, the mechanical property of this AC gel (0.2 mM) also exhibited enhanced tensile strength compared to void A gel justifying its potential to be used for wound healing base. Figure 1(f) reveals that the petals of the nanoflowers are 220 nm in length and 30–75 nm in width, whereas the AC scaffold (synthesized from 0.2 mM of cerium nitrate) was 750–800 nm in size. It was believed that with reaction time, the nanopetals of AC gels were self-assembled into a flower-like architecture by the forced compact structure of plenty of –OH functionalities on CNP nanocrystal surfaces [45–47]. The nanoflower-like architecture of AC gel was quite similar to the previously reported literature [48] where in the presence of ceric ions, acrylamide and glucose molecules copolymerized to fabricate CNP-embedded gel network. It was speculated that Ce^{3+} was oxidized to $Ce(OH)_4$ by peroxide radicals which further dehydrated to form CeO_2-entrapped A gel or AC gel as previously observed in the case of ZnO nanoflowers [49]. These AC gels with three different cerium concentrations (0.1, 0.2, and 0.2 mM) (data not shown) were evaluated for curcumin entrapment to find out the best scaffold for our experiment. The highest drug entrapment was obtained in AC gel of 0.2 mM concentration which was anticipated due to its uniform and compact nanoflower with highly ordered porous architecture. Therefore, for the rest of this study, AC gel (with 0.2 mM entrapped CNPs) has been utilized as the final scaffold for curcumin loading. After the fabrication of ACC gels, the scaffold was also characterized through TEM analysis. TEM images of ACC scaffold (Fig. 1j, k) showed the same nanoflower-like morphology with each of the petals being around 220–240 nm in size. The synthesized control AC' scaffold (curcumin-loaded A gels) was also visualized through TEM analysis, and it was observed that the image (Fig. S6) displayed the spherical morphology of nanogels (each sphere is 35–40 nm in size) which was completely different from ACC morphology. It could be inferred that the ambiguity between the morphology between ACC and AC' gels was due to the in situ formation of CNP inside the microstructure which controls the nanoflower-like morphology of desired ACC gel [45, 46, 48, 49].

The FT-IR spectra of A, AC, and ACC scaffolds are shown in Fig. S7. FTIR spectrum of void A gel shows characteristic peaks of both poly (acrylamide) and AMPS between 3300 and 3500 cm^{-1} (stretching vibrations of $–OH/–NH_2$), 1647 cm^{-1}(stretching vibration of C=O of PAAm) and 1124–1038 cm^{-1} (absorption of peak of $-SO_3H/-SO_3Na$ of AMPS unit) [4] whereas AC hydrogel exhibited similar peaks with a slight red shift change in their vibrational frequencies, confirming the presence of CNP [40]. In the final ACC scaffold, additional peaks are observed at 1500 cm^{-1} and 1275 cm^{-1} due to characteristic peaks of curcumin. The FT-IR data of control AC' gel was also recorded to verify curcumin entrapment, and similar peaks due to curcumin with little shifts were observed in AC' gel (given as Fig. S8 in the supporting information).

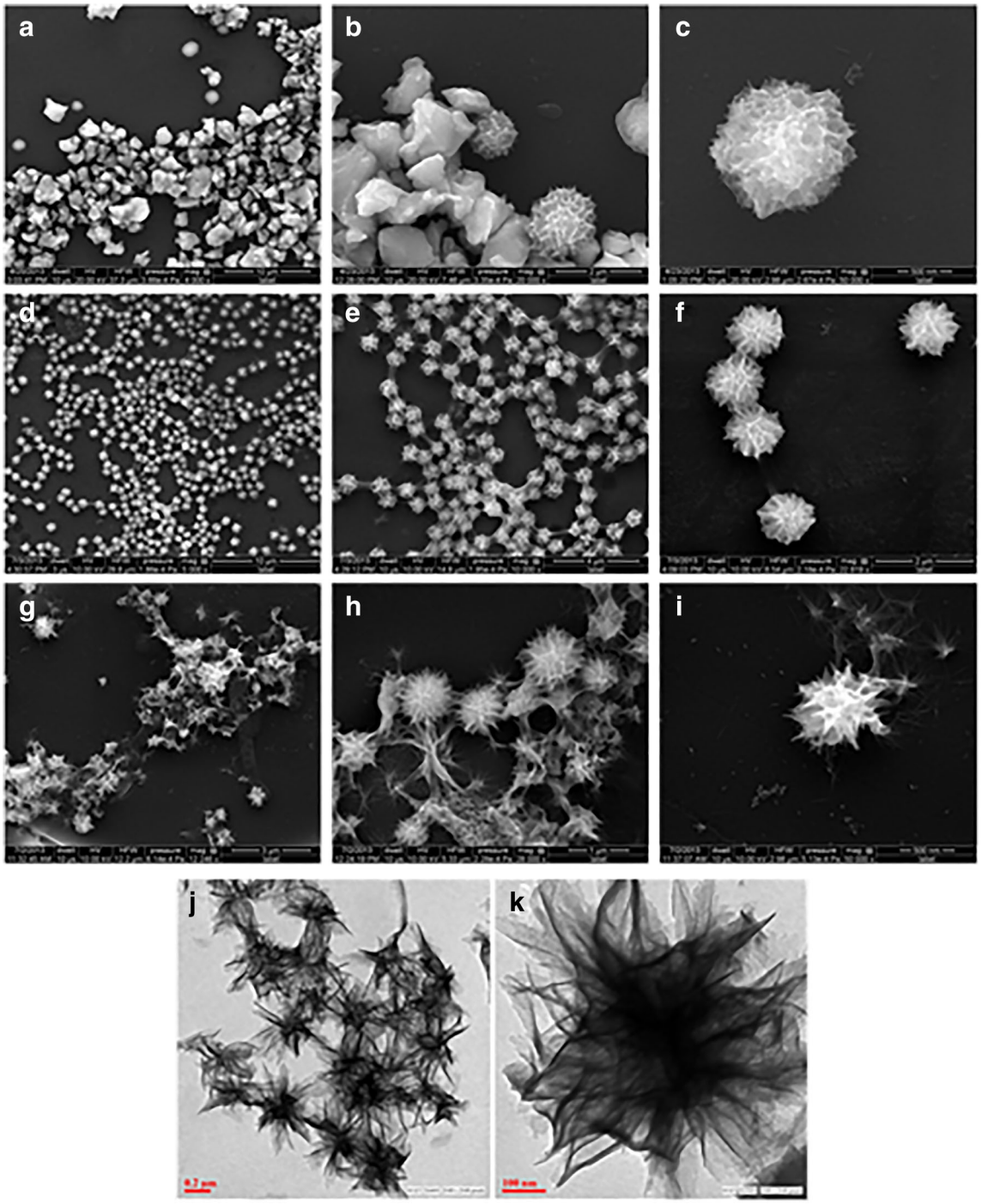

Fig. 1 Characterization of AC gels via scanning electron microscopy (SEM) and transmission electron microscopy (TEM). **a**–**c** Images of 0.1 mM CeO_2 entrapped AC gels at different magnifications. **d**–**f** Images of 0.2 mM CeO_2 entrapped AC gel. **g**–**i** Images of 0.4 mM CeO_2-entrapped AC gel. **j**, **k** Transmission electron microscopy (TEM) images of ACC gels at different magnifications

In vitro evaluation of dressing scaffolds via drug release and cytotoxicity studies

To establish the efficiency of ACC gel as an efficient drug delivery system, a sustained and slow release of curcumin from ACC scaffold is mainly important for complete remedy. In this view, the DL and EE of ACC scaffold were found as $4.64 \pm 0.5\%$ and $77 \pm 0.3\%$, respectively. In the in vitro release profile (Fig. S9) of ACC, the biphasic release pattern indicated an improved release profile than AC' gel, followed by a gradual and sustained release of $85 \pm 7.5\%$ over 6 days which matched well with the previously reported literature [16]. However, the release of curcumin from AC' gel was also conducted but it displayed a comparatively higher burst

release profile in the first 24 h (59 ± 7.17%) than ACC (46% in the first 24 h), and after 6 days, almost 95% of drug was released from AC' gel. This controlled release profiling of curcumin from ACC was assumed due to the CNP-entrapped microstructure (nanoflower-like morphology), which controls the higher DL, EE, and sustained release of the drug over 6 days. Thus, the designed ACC scaffold would be more potent as a sustained drug release system as well as a wound healing material. In addition, we also tested the biocompatibility of the synthesized A, AC', AC, and ACC scaffolds using the HaCaT cells for 24 h. As HaCaT cells are human keratinocytes from skin origin, they possess both regulatory and secretory functions, so the biocompatibility of our wound healing agents was studied using HaCaT cells. From the results of MTT assay, it was evident that the cells treated with ACC, AC, A, and AC' scaffolds have shown profound biocompatibility up to 500 μg/ml. Even at 500 μg/ml of ACC scaffold containing 23.2 μg of curcumin, no change was observed in the viability and proliferating ability of human aneuploid immortal keratinocytes (Fig. S10).

Analysis of wound healing efficacy of various gels in an animal model

To evaluate whether the combination of CNP and curcumin provides a better healing environment, we compared the efficacy of all combinations (AC, AC', ACC) in wound dressing scaffolds. These scaffolds were applied to a full-thickness open excision acute wound model in male Wistar rats, and their efficacy was compared with commercial dressing (B, Medicare sterilized adsorbent cotton) and dressings containing only curcumin or CNP (shown in Fig. S11). After creating 10-mm wounds via surgery, all the synthesized scaffolds (A, AC, AC', ACC) and commercial wound dressing B were applied to wound region for a period of 3, 7, and 14 days. At day 3, after application, no significant difference in healing (data not shown) was observed. Therefore, wound closure was analyzed in each group as a percentage of recovery of the wounded area at days 7 and 14. At each time points (7th and 14th days), wounds were opened and analyzed. It is already reported that re-epithelialization of the wound surface takes place mostly through the basal epithelial cell migration by the edges of the wound [50, 51]. Scab formation around the edges of the wound at 7 days post injury in ACC-treated group was minimal compared to other treated groups. At day 14, clear and visible patches of hair regrowth was found in the ACC group, suggesting a greater degree of healing. As seen in Fig. 3, ACC-treated animals consistently showed higher wound closure rate (~ 78%), as compared to the wound closure rates in AC' (~ 51.11%), AC (~ 46%), A (~ 32%), and B (~ 13%) groups on the 7th day. On the 14th post wounding day, no visible wound was present in ACC due to coverage with hair while other groups had different levels of open wounds. Both AC- and AC'-treated groups showed almost 90–95% healing. From the Tukey's test, the 7th day wound closure rates for desired ACC with AC' showed very high-quality statistical significance $p < 0.001$ (***) while the same healing pattern after 14 days exhibited a high-quality statistical significance with a $p < 0.01$ (**). Therefore, it can be considered that the desired ACC would be a potent scaffold towards wound healing applications. The efficacy of AC over A was also checked through comparing the 7th and 14th day healing capacity with a high-quality statistical significance ($p < 0.01$**) indicating the motivation of using CNP in A hydrogel. Therefore, as evident from the images (Fig. 2) as well as from the wound healing results (Fig. 3), a single application of ACC scaffold promotes almost complete healing (99%) as compared to AC' (93%) and AC (89%) after the 14th day of application. In earlier studies on curcumin-based dressings [4, 17], there was a sufficient amount of scar tissue remaining in the wound after 14 days post wounding. Similarly, an isolated study of CNPs and wound healing had earlier demonstrated that even after daily application till 13 days, there was incomplete repair of the wound [1]. In our case, from EDX data (Fig. S12), it was demonstrated that a single application of our ACC scaffold comprising of much lower amount of CNP (87.21 μM) could efficiently heal the scar as compared to the previous reported daily dose (130 μM) [1]. These studies indicate that the fabricated ACC bandage with 87.21 μM CNP and 23.2 mg curcumin (calculated from EDX analysis and drug loading amount) is a better wound healing scaffold exhibiting superior healing compared to the previously reported curcumin- or CNP-based dressings [1, 4, 17]. This enhanced activity is largely due to the combined effects of CNP and curcumin, thus promoting rapid wound closure. Rapid wound closure and resolution of inflammation also prevented wounds from becoming chronic suggesting a significant beneficial effect of an optimal combination of curcumin and CNP. In models of chronic wounds, there may be a need to apply this combination multiple times but at low doses. This could be studied in the future.

Histopathological analysis for wound repair and deposition of extracellular matrix components

For histopathology and special staining, skin sections from each group at different time points were stained with hematoxylin and eosin (H&E) for general observation of skin damage. Sections were also stained with Masson's trichrome (MT) blue staining to study the pattern of collagen deposition in the healed tissue. Figure 4 shows histopathological investigations of the wounds treated with ACC, AC', AC, and A scaffolds

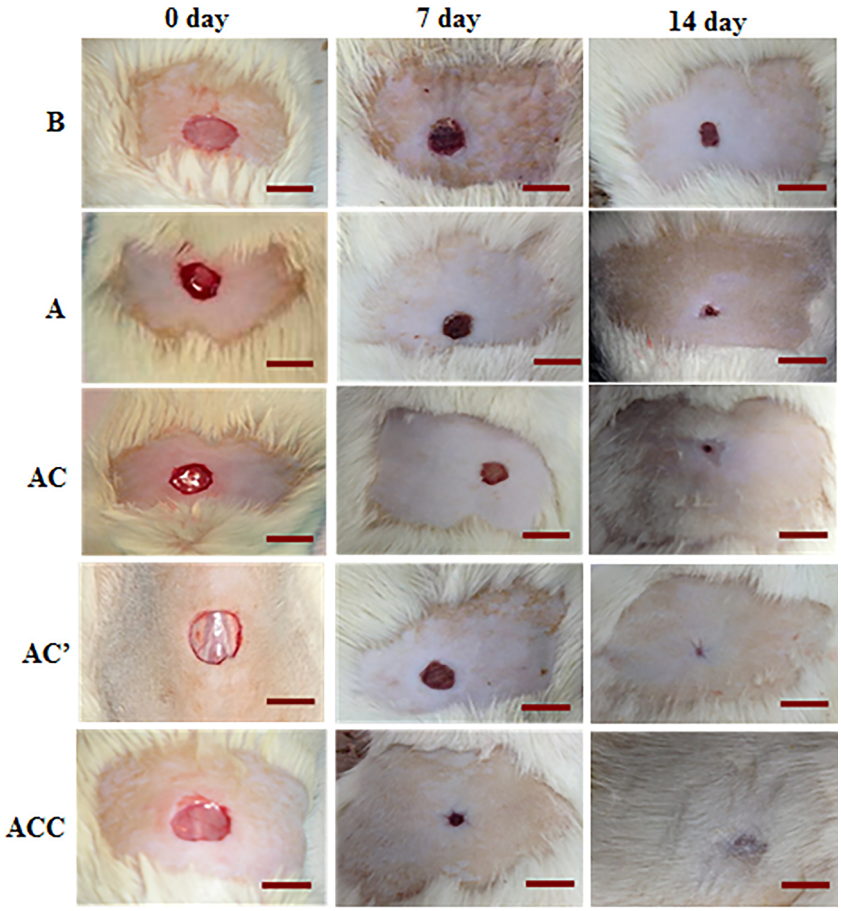

Fig. 2 Wound healing efficacy of different scaffolds. Photographs of wounds treated with commercial bandage (B), acrylamide (A) gel, CeO_2-A (AC) gel, curcumin-A gel (AC'), and curcumin-CeO_2-A gel (ACC) scaffolds at different postoperative days (0, 7, and 14). Red bar represents 10 mm

and commercial dressing B at different time intervals. On the 7th postoperative day, commercial scaffold-treated group B and A treated groups still had higher amount of necrotic cells and scabbing of the wound, while AC and AC' showed later stages of healing with complete removal of scabbed tissue and necrotic cells. In contrast, the combined treatment group ACC showed new epidermal layer formation and organized dermis. Astonishingly, some isolated nascent hair follicles also appeared in the ACC-treated animals. At 14 days, wound closure was evident across all the groups, but animals from groups A,

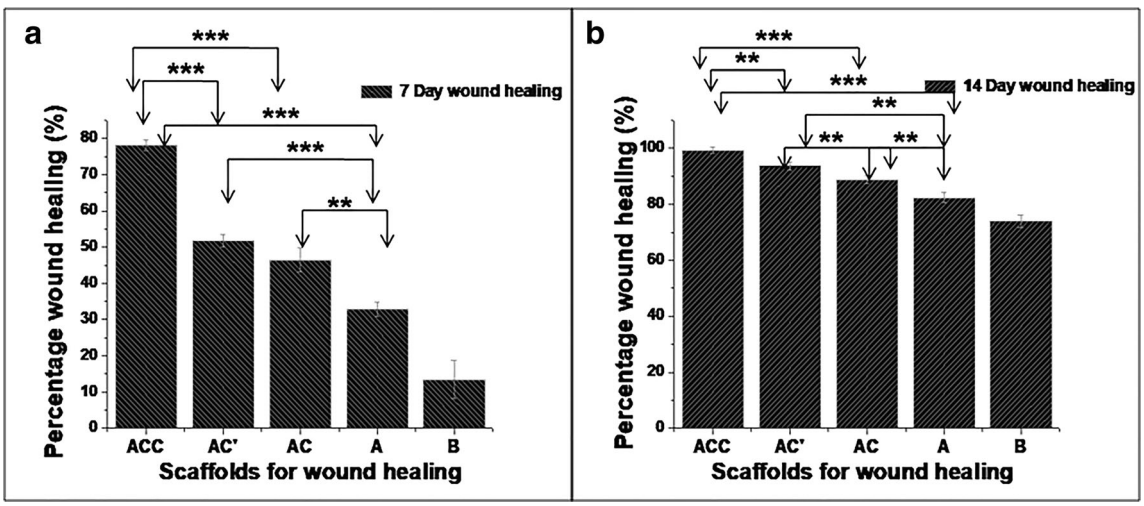

Fig. 3 Closure of wounds over time represented as a percent wound healing. **a** Percentage wound healing after treatment with ACC, AC', AC, A, and B scaffolds at 7th postoperative day. **b** Percentage wound healing after treatment with ACC, AC', AC, A, and B scaffolds at 14th postoperative day. Values of $*p < 0.05$, $**p < 0.01$, and $***p < 0.001$ (ANOVA with Tukey's multiple comparison test) were indicative of statistically significant differences

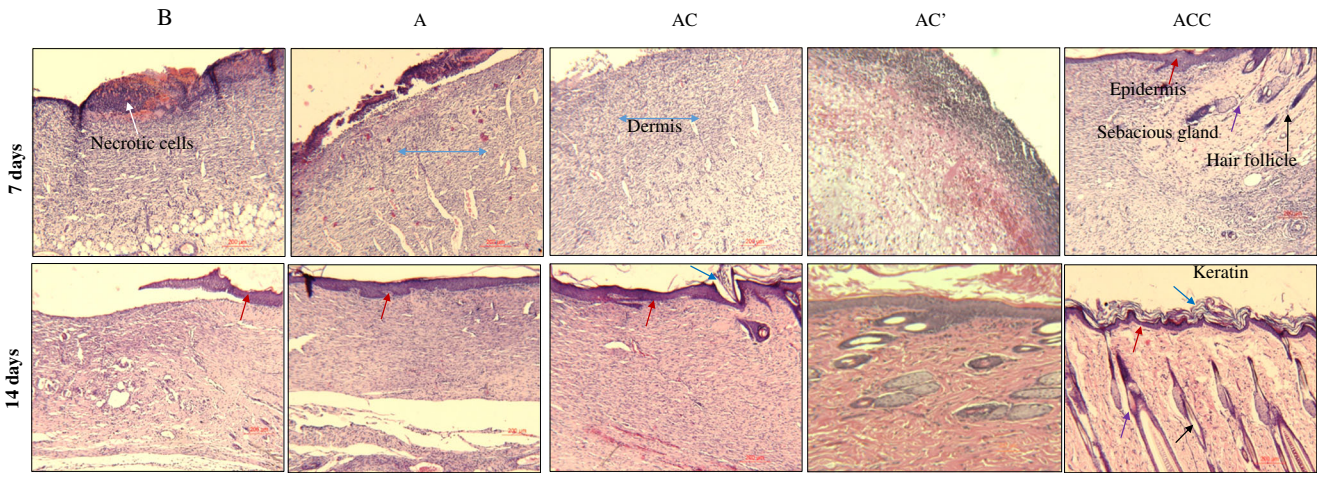

Fig. 4 Histological study showing the effect of B, A, AC, AC', and ACC scaffolds on wound healing in rats at different postoperative days (7th (7) and 14th (14) days). Increased formation of epidermis, sebaceous glands, hair follicles, and dermis can be seen in the ACC group at day 14. Appearance of keratin can be seen on the 14th postoperative days in ACC-, AC'-, and AC-treated wounds. Representative light microscopy photographs of tissue sections are presented for all five groups. Bar length 200 μm

B, and AC showed the presence of high numbers of leucocyte infiltrate, suggesting slower resolution of inflammation from the wound healing process. While the differentiation of epidermal and dermal layers was visible, no nascent hair follicles were seen in the deep dermis. Interestingly, in the combined treatment group ACC, we observed full resolution of wound as well as less inflammation with no leucocyte infiltrate. Interestingly on the 14th day, ACC-treated group showed well-formed epidermis, properly arranged dermis, and enhanced re-epithelialization of the wound with properly arranged hair follicles and sebaceous glands which is almost similar with normal skin morphology. More interestingly, ACC-treated groups showed well-formed keratin layers in the repaired skin whereas in AC' and AC groups, keratin appeared in trace amount and in A group was almost negligible.

Furthermore, it is known that during new tissue formation, the local accumulation and structured organization of collagen strongly correlates with the accretion of tensile strength and indicative of the proper progression of healing process [52]. Therefore, the organization of tissues at the wounded area and extent of structural collagen deposition [53, 54] in the wounds was examined by Masson's trichrome staining. From the stained tissue sections, it was demonstrated that the ACC scaffold resulted in greater amount of well-structured collagen deposition in the wounds as compared to AC', AC, A, and control B treated wounds on the 7th as well as 14th post-wounding days (Fig. 5).

Effect of different scaffolds on the expression of growth-related proteins

To further understand the underlying mechanisms responsible for accelerated and scarless wound healing, we performed cytokine profiling and multiplex analysis for proteins involved in various cell signaling pathways related to wound repair in animals. A substantial increase in the expression of growth- and repair-related cytokines (IL6, IL10, and IL13) was also observed. There was a robust expression of IL6 and IL13 at day 14 post wounding in ACC-treated groups (Fig. 6a) with concomitant increase in expression of anti-inflammatory IL10 gene [55]. Increased expression of growth as well as proliferation factors such as TGF-β (transforming growth factor) [56] and VEGFR (vascular endothelial growth factor receptor) [57] was observed in all the five groups (Fig. 6c–d). Interestingly, MCP-1 (monocyte chemotactic protein-1) [55] was only expressed to high levels in the ACC group. MCP-1 plays an important role in promoting angiogenesis acting synergistically with VEGF [58] and TGF-β [56]. MCP-1 has been shown to be crucial for wound re-epithelialization, angiogenesis, and recruitment of alternatively activated macrophages (AAM) which promote healing [55]. As seen in Fig. 6b, MCP-1 showed a very robust expression only in the ACC group. The 7th and 14th day post-wounding tissue treated with ACC scaffold showed more organized collagen deposition, suggesting the early influx of fibroblasts towards the wound and enhanced collagen deposition [6, 52–54].

TGF-β also showed sequentially increased expression in tissues treated with control B, A, AC', AC, and ACC scaffolds (Fig. 6c). During the early stage of wound healing, the expression of TGF-β would promote the migration of resident dermal fibroblasts towards the wound site, followed by extracellular matrix reorganization. This process eventually results in skin tissue regeneration and wound contraction. As shown in Fig. 6d, VEGF receptor VEGFR2 expression demonstrated an increasing trend with maximum expression in ACC scaffold-treated tissues. The expression of VEGFR2 in the ACC group displayed the highest

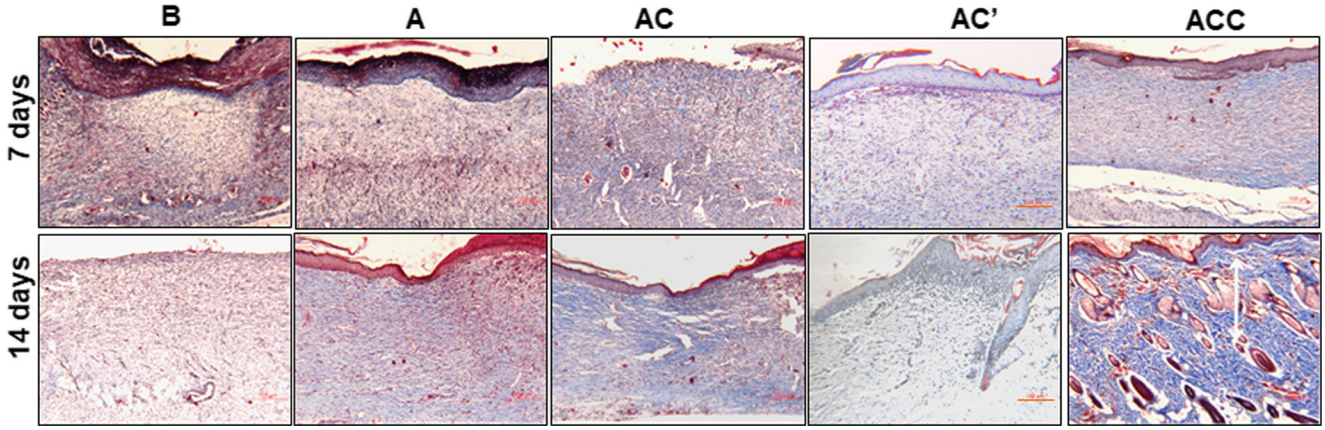

Fig. 5 Masson's trichrome staining for detection of collagen in wound tissue treated with B, A, AC, AC', and ACC scaffolds at the 7th (7) and 14th (14) days post wounding. Representative light microscopy photographs of tissue sections are presented for all five groups. Increased deposition of well-organized collagen is seen in healed areas of ACC group. Bar length 200 μm

level during the overall observation suggesting increased angiogenesis and tissue growth at the site of injury.

Previous studies of wound healing have demonstrated that the expression of key growth factors related to wound healing, such as VEGF and TGF-β, are vital in the maturation of full-thickness wounds [58, 59]. They can also enhance angiogenesis by increasing the production of VEGF and decreasing redox-dependent apoptosis and increase cell viability [60]. VEGF and PDGF belong to the family of platelet-derived growth factors, which induce angiogenesis, endothelial cell proliferation as well as stimulate epithelialization, collagen deposition and vascular permeability [61]. TGF-β is also known

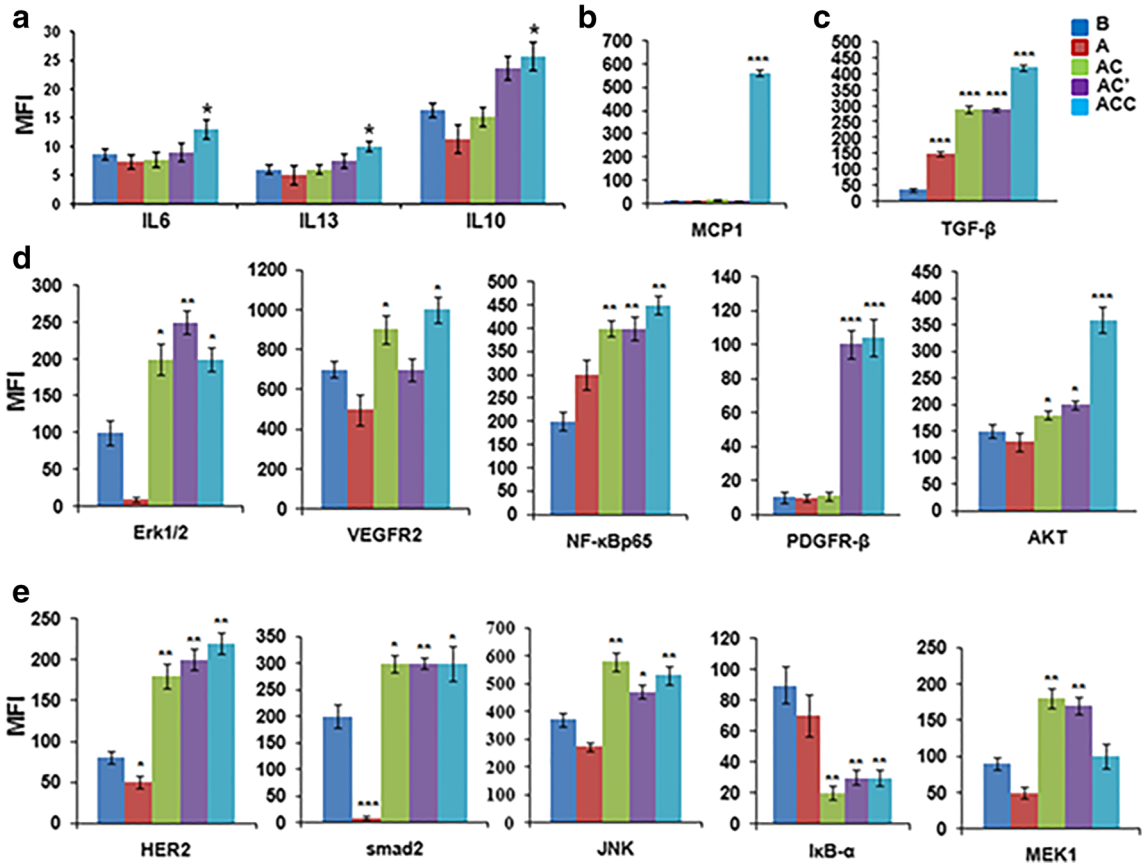

Fig. 6 Identification of genes and cell signaling proteins involved in wound repair, growth, and differentiation. **a**, Cytokine profiling in serum obtained from animals. **b** MCP-1 expression at day 14 in all the five groups. **c** Expression of TGF-β at day 14 in all groups. **d**, **e** Identification of total and phosphorylated proteins involved in cell signaling. Tissue lysate from day 14 wound area was used for the profiling. ***$p < 0.001$, **$p < 0.01$, *$p < 0.05$ as compared to **B** ($n = 6$ rats per group). Data is represented as mean ± SD

to be a potent stimulator of fibroblast proliferation and collagen synthesis as well as accelerating re-epithelialization and enhancing wound healing [62].

Upon induction with TGF-β, the activity of MCP-1 is enhanced with increasing recruitment of cells at the site of injury, but at a later stage, it promotes wound re-epithelialization, angiogenesis, and collagen synthesis. MCP-1 also promotes differentiation of alternatively activated macrophages [63]. Unlike classically activated macrophages, these macrophages play a key role in maintaining homeostasis and promoting wound repair [64]. They could, therefore, form the major pool of inflammatory cells seen in ACC groups and also account for accelerated repair instead of injury induced by classical inflammatory cells. Studies using MCP-1 knockout mice have shown delayed re-epithelialization, angiogenesis, and collagen synthesis, suggesting its crucial role in wound healing [65].

Activation of key cell signaling proteins and pathways involved in wound healing

There are very few studies defining the underlying mechanisms and role of upstream and downstream mediators associated with the promotion of wound repair. After identifying the classical markers of wound repair such as TGF-β and

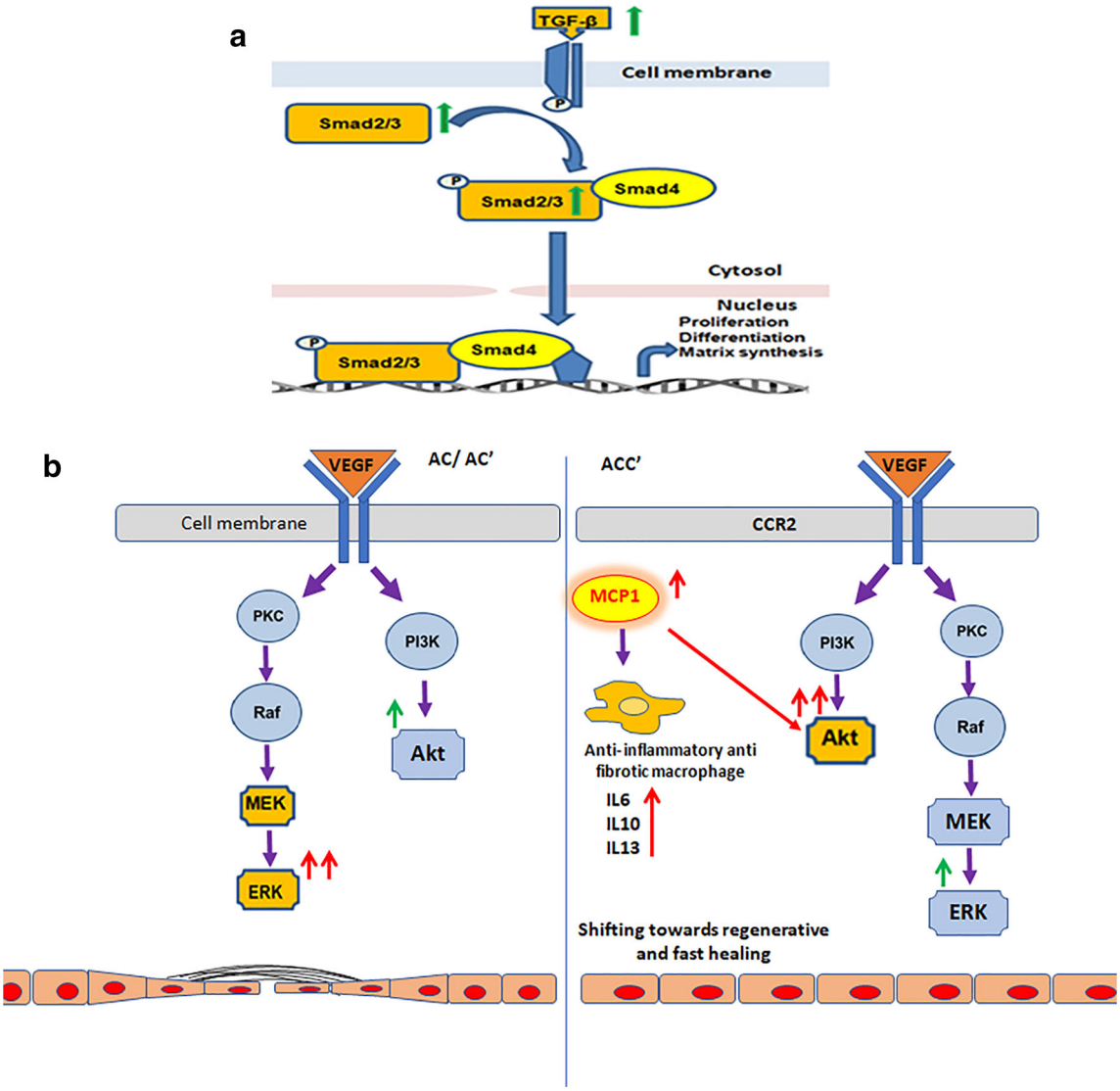

Fig. 7 Proposed mechanisms for action of various proteins involved in wound repair which were identified in this study. Arrows represent the proteins identified in our study which show increased or decreased expression/phosphorylation. **a** Role of TGF-β and the downstream smad2 proteins. Binding of TGF-β to its receptor leads to downstream activation of Smad2/3 signaling proteins which are then translocated to nucleus. Smads then induce the expression of multiple genes involved in growth, proliferation, and matrix synthesis by binding to their regulatory regions. **b** Diagram shows different cell signaling pathways activated in ACC and AC/AC' group by increased protein production and phosphorylation and their effect on growth and repair. Binding of growth factors leads to activation of MAPK/ERK related to growth and differentiation in the AC, AC', and ACC groups. However, the ACC group shows selective hyperactivation of AKT pathway which then stimulates MCP1 expression and promotes faster wound healing and complete regeneration

MCP-1, we had done studies to identify the upstream initiators and downstream effectors which are responsible for accelerated healing seen in the animals treated with ACC formulation. Studies were done to identify total and phosphorylated proteins involved in the regulation of signaling pathways associated with wound repair. Our study shows that the ACC formulation accelerated wound healing in this rat model by activating the proteins involved in TGF-β-VEGF-MCP-1 and TGF-β-Smad2 signaling [65]. There was a significant increase in phosphorylation of Erk1/2, VEGFR-2, NF-κBp65, PDGFR-β, and AKT (Fig. 6d), which varied from 2 to 5 folds. There was also a marked increase in total protein concentration of HER2, Smad2, JNK, and MEK1 and decrease in IκB-α (Fig. 6e). All these proteins play a significant role in the activation and downstream signaling of HER2/ErbB2 pathway. HER2 or ErbB2 is the high affinity epidermal growth factor receptor [66] which plays a crucial role in embryonic development [67]. It can also induce angiogenesis through VEGF stimulation [68] and promote wound repair [69–71]. Our study also shows increased VEGF production which may lead to the activation of downstream signaling responsible for increased endothelial cell survival, migration, and proliferation. Production of VEGF is associated with the activation of VEGFR2 receptor and other downstream signaling mediators seen in our study such as Akt, MEK, and ERK, thereby activating the MAPK pathway. Increased TGF-β production (Fig. 7a) could also lead to increased phosphorylation of the downstream Smad2 to promote accelerated wound repair in animals treated with the ACC formulation. Taken together, our study shows that the optimum combination of curcumin and CNPs in the ACC hydrogel formulation acts as a potent inducer of MCP1 and TGF-β cascade of signaling pathways and mediators which reduce inflammation, activate Type 2 macrophages, cell survival genes, and growth factors (Fig. 7b). This leads to a near complete healing of cutaneous wounds at an accelerated rate with minimal scarring around the wound area.

Conclusions

An optimal combination was developed in which anti-inflammatory curcumin and antioxidant nanoparticle CNP are combined in a hydrogel scaffold-based (ACC) dressing. This dressing was thoroughly investigated via physicochemical and biological techniques to evaluate its efficacy in a topical wound healing model in Wistar rats. The hydrogel matrix facilitated the sustained release of the encapsulated curcumin (> 85% in 6 days) from the CNP-entrapped ACC scaffold, and at the same time, the antioxidant property of CNP also acts to promote the accelerated and scarless healing. This led to early resolution of inflammation, complete wound closure, and regrowth of hair follicles in the ACC group through selective activation of factors such as MCP-1. Only a single application of ACC scaffold was sufficient to promote complete healing. Further studies could be done via adding an antibacterial agent and a more potent pro-angiogenic component in this formulation to provide even higher wound healing efficacy.

Acknowledgements D. Bhattacharya acknowledges support (GAP 267) from the Nano-Mission of Department of Science and Technology (DST), New Delhi, India, for providing funding and Postdoctoral Fellowship. KCG thanks ICMR, N.Delhi, for awarding Dr. A.S.Paintal Distinguished Scientist Chair to him. Authors gratefully acknowledge the financial support (GAP 224) from the Department of Science and Technology (DST), New Delhi, India, and CSIR Network Grant NANOSHE (BSC0112, DBT GAP-302). We also thank our Director Prof. Alok Dhawan for all the help and support. Authors are also thankful to Dr. P.N.Saxena and Miss N. Argaria, CSIR-IITR for SEM and TEM analysis and IIT Kharagpur, for the use of their sophisticated instrumentation facility (XRD and FTIR). Authors also acknowledge a kind gift of HaCaT cells from Dr. R. S. Ray (CSIR-IITR).

Compliance with ethical standards

Conflict of interest The authors declare no competing financial interest.

References

1. Chigurupati S, Mughal MR, Okun E, Das S, Kumar A, McCaffery M, et al. Effects of cerium oxide nanoparticles on the growth of keratinocytes, fibroblasts and vascular endothelial cells in cutaneous wound healing. Biomaterials. 2013;34:2194–201.
2. Lee J, Wang YL, Ren F, Lele TP. Stamp wound assay for studying coupled cell migration and cell debris clearance. Langmuir. 2010;26:16672–6.
3. Tran NQ, Joung YK, Lih E, Park KD. In situ forming and rutin-releasing chitosan hydrogels as injectable dressings for dermal wound healing. Biomacromolecules. 2011;12:2872–80.
4. Mohanty C, Das M, Sahoo SK. Sustained wound healing activity of curcumin loaded oleic acid based polymeric bandage in a rat model. Mol Pharm. 2012;9:2801–11.
5. Gopinath D, Ahmed MR, Gomathi K, Chitra K, Sehgal PK, Jayakumar R. Dermal wound healing processes with curcumin incorporated collagen films. Biomaterials. 2004;25:1911–7.
6. Leu JG, Chen SA, Chen HM, Wu WM, Hung CF, Yao YD, et al. The effects of gold nanoparticles in wound healing with antioxidant epigallocatechin gallate and α-lipoic acid. Nanomedicine. 2012;8:767–75.
7. Panchatcharam M, Miriyala S, Gayathri V, Suguna L. Curcumin improves wound healing by modulating collagen and decreasing reactive oxygen species. Mol Cell Biochem. 2006;29:87–96.
8. Choi JK, Jang JH, Jang WH, Kim J, Bae IH, Bae J, et al. The effect of epidermal growth factor (EGF) conjugated with low-molecular-weight protamine (LMWP) on wound healing of the skin. Biomaterials. 2012;33:8579–90.
9. Naksuriya O, Okonogi S, Schiffelers RM, Hennink WE. Curcumin nanoformulations: a review of pharmaceutical properties and preclinical studies and clinical data related to cancer treatment. Biomaterials. 2014;35:3365–83.
10. Ruby AJ, Kuttan G, Dinesh KB, Rajasekharan KN, Kuttan R. Anti-tumour and antioxidant activity of natural curcuminoids. Cancer Lett. 1995;94:79–83.

11. Jagetia G, Aggarwal BB. "Spicing up" of the immune system by curcumin. J Clin Immunol. 2007;27:19–35.
12. Tang H, Murphy CJ, Zhang B, Shen Y, Van Kirk EA, Murdoch WJ, et al. Curcumin polymers as anticancer conjugates. Biomaterials. 2010;31:7139–49.
13. Yallapu MM, Jaggi M, Chauhan SC. Curcumin nanoformulations: a future nanomedicine for cancer. Drug Discov Today. 2012;17:71–80.
14. Sidhu GS, Mani H, Gaddipati JP, Singh AK, Seth P, Banaudha KK, et al. Curcumin enhances wound healing in streptozotocin induced diabetic rats and genetically diabetic mice. Wound Repair Regen. 1999;7:362–74.
15. Phan TT, See P, Lee ST, Chan SY. Protective effects of curcumin against oxidative damage on skin cells in vitro: its implication for wound healing. J Trauma Acute Care Surg. 2001;51:927–31.
16. Chereddy KK, Coco R, Memvanga PB, Ucakar B, des Rieux A, Vandermeulen G. Préat, V Combined effect of PLGA and curcumin on wound healing activity. J Control Release. 2013;171:208–15.
17. Gong CY, Wu QJ, Wang YJ, Zhang DD, Luo F, Zhao X, et al. A biodegradable hydrogel system containing curcumin encapsulated in micelles for cutaneous wound healing. Biomaterials. 2013;34:6377–87.
18. Dai, M.; Zheng, X.L.; Xu, X.; Kong, X.Y.; Li, X.Y.; Guo, G.; Luo, F.; Zhao, Quan Wei, X.Y.; Qian, Z. Chitosan-alginate sponge: preparation and application in curcumin delivery for dermal wound healing in rat. J Biomed Biotechnol 2009, 2009, 595126–595134.
19. Xu C, Qu X. Cerium oxide nanoparticle: a remarkably versatile rare earth nanomaterial for biological applications. NPG Asia Mater. 2014;6:e90–e106.
20. Perez JM, Asati A, Nath S, Kaittanis C. Synthesis of biocompatible dextran-coated nanoceria with pH-dependent antioxidant properties. Small. 2008;4:552–6.
21. Asati A, Santra S, Kaittanis C, Nath S, Perez JM. Oxidase-like activity of polymer-coated cerium oxide nanoparticles. Angew ChemInter Ed. 2009;48:2308–12.
22. Celardo I, Pedersen JZ, Traversa E, Ghibelli L. Pharmacological potential of cerium oxide nanoparticles. Nanoscale. 2011;3:1411–20.
23. Xu C, Lin Y, Wang J, Wu L, Wei W, Ren J, et al. Nanoceria-triggered synergetic drug release based on CeO_2-capped mesoporous silica host–guest interactions and switchable enzymatic activity and cellular effects of CeO_2. Adv Health Mater. 2013;2:1591–9.
24. Mandoli C, Pagliari F, Pagliari S, Forte G, Nardo PD, Licoccia S, et al. Stem cell aligned growth induced by CeO_2 nanoparticles in PLGA scaffolds with improved bioactivity for regenerative medicine. Adv Funct Mater. 2010;20:1617–24.
25. Chen J, Patil S, Seal S, McGinnis JF. Rare earth nanoparticles prevent retinal degeneration induced by intracellular peroxides. Nat Nanotechnol. 2006;1:42–50.
26. Tarnuzzer RW, Colon J, Patil S, Seal S. Vacancy engineered ceria nanostructures for protection from radiation-induced cellular damage. Nano Lett. 2005;5:2573–7.
27. Niu J, Azfer A, Rogers L, Wang X, Kolattukudy P. Cardioprotective effects of cerium oxide nanoparticles in a transgenic murine model of cardiomyopathy. Cardiovasc Res. 2007;73:549–59.
28. Rather HA, Thakore R, Singh R, Jhala D, Singh S, Vasita R. Antioxidative study of cerium oxide nanoparticle functionalised PCL-gelatin electrospun fibers for wound healing application. Bioactive Materials. 2017, *xxx*:1–11.
29. Anumolu SS, Menjoge AR, Deshmukh M, Gerecke D, Stein S, Laskin J, et al. Doxycycline hydrogels with reversible disulfide crosslinks for dermal wound healing of mustard injuries. Biomaterials. 2011;32:1204–17.
30. Smithmyer ME, Sawicki LA, Kloxin AM. Hydrogel scaffolds as *in vitro* models to study fibroblast activation in wound healing and disease. Biomater Sci. 2014;2:634–50.
31. Jayakumar R, Menon D, Manzoor K, Nair SV, Tamura H. Biomedical applications of chitin and chitosan based nanomaterials—a short review. Carbohydr Polym. 2010;82:227–32.
32. Zhu J, He P, Lin L, Jones DR, Marchant RE. Biomimetic poly(ethylene glycol)-based hydrogels as scaffolds for inducing endothelial adhesion and capillary-like network formation. Biomacromolecules. 2012;13:706–13.
33. Murali R, Thanikaivelan P, Cheirmadurai K. Melatonin in functionalized biomimetic constructs promotes rapid tissue regeneration in Wistar albino rats. J Mater Chem B. 2016;4:5850–62.
34. Dumitriu RP, Profire L, Nita LE, Dragostin OM, Ghetu N, Pieptu D, et al. Chitosan conjugates and their polyelectrolyte complexes with hyaluronate destined to the management of burn wounds. Materials. 2015;8:317–38.
35. Durmaz S, Okay O. Acrylamide/2-acrylamido-2-methylpropane sulfonic acid sodium salt-based hydrogels: synthesis and characterization. Polymer. 2000;41:3693–704.
36. Su E, Okay O. Hybrid cross-linked poly(2-acrylamido-2-methyl-1-propanesulfonic acid) hydrogels with tunable viscoelastic, mechanical and self-healing properties. React Funct Polym. 2018;123:70–9.
37. Han IK, Sang PJ, Jeong KS. Volume behavior of interpenetrating polymer network hydrogels composed of polyacrylic acid-co-poly(vinyl sulfonic acid)/polyaniline as an actuator. Smart Mater Struct. 2006;15:1882–6.
38. Lu Y, Mei Y, Drechsler M, Ballauff M. Thermosensitive core–shell particles as carriers for ag nanoparticles: modulating the catalytic activity by a phase transition in networks. Angew Chem Int Ed. 2006;45:813–6.
39. Lu Y, Ballauff M. Thermosensitive core-shell microgels: from colloidal model systems to nanoreactors. Prog Polym Sci. 2011;36:767–92.
40. Saravanan P, Raju MP, Alam S. A study on synthesis and properties of Ag nanoparticles immobilized polyacrylamide hydrogel composites. Mater Chem Phys. 2007;103:278–82.
41. Varaprasad K, Mohan YM, Vimala K, Raju KM. Synthesis and characterization of hydrogel-silver nanoparticle-curcumin composites for wound dressing and antibacterial application. J App Polym Sc. 2011;121:784–96.
42. Chopra D, Ray L, Dwivedi A, Tiwari SK, Singh J, Singh KP, et al. Photoprotective efficiency of PLGA-curcumin nanoparticles versus curcumin through the involvement of ERK/AKT pathway under ambient UV-R exposure in HaCaT cell line. Biomaterials. 2016;84:25–41.
43. Lee CH, Hsieh MJ, Chang SH, Lin YH, Liu SJ, Lin TY, et al. Enhancement of diabetic wound repair using biodegradable nanofibrous metformin-eluting membranes: in vitro and in vivo. ACS Appl Mater Interfaces. 2014;6:3979–86.
44. Han L, Xu J, Lu X, Gan D, Wang Z, Wang K, et al. Biohybrid methacrylated gelatin/polyacrylamide hydrogels for cartilage repair. J Mater Chem B. 2017;5:731–41.
45. Yissar VP, Gabai R, Shipway AN, Bourenko T, Willner I. Gold nanoparticle/hydrogel composites with solvent-switchable electronic properties. Adv Mater. 2001;13:1320–3.
46. Li GR, Qu DL, Arurault L, Tong YX. Hierarchically porous Gd^{3+}-doped CeO_2 nanostructures for the remarkable enhancement of optical and magnetic properties. J Phys Chem C. 2009;113:1235–41.
47. Sinha AK, Jana S, Pande S, Sarkar S, Pradhan M, Basu M, et al. New hydrothermal process for hierarchical TiO_2 nanostructures. CrystEngComm. 2009;11:1210–2.
48. Sun C, Sun J, Xiao G, Zhang H, Qiu X, Li H, et al. Mesoscale organization of nearly monodisperse flowerlike ceria microspheres. J Phys Chem B. 2006;110:13445–52.

49. Dai S, Li Y, Du Z, Carter KR. Electrochemical deposition of ZnO hierarchical nanostructures from hydrogel coated electrodes. J Electrochem Soc. 2013;160:D156–62.
50. Kumar, V.; Abbas, A.; Fausto, N. Robbins & Cotran Pathologic Basis of Disease, Seventh Edition. ISBN-13: 978–0721601878.
51. Li X, Chen S, Zhang B, Li M, Diao K, Zhang Z, et al. In situ injectable nano-composite hydrogel composed of curcumin, N,O-carboxymethyl chitosan and oxidized alginate for wound healing application. Int J Pharm. 2012;437:110–9.
52. Heckert EG, Karakoti AS, Seal S, Self WT. The role of cerium redox state in the SOD mimetic activity of nanoceria. Biomaterials. 2008;29:2705–9.
53. Tsai YM, Chien CF, Lin LC, Tsai TH. Curcumin and its nano-formulation: the kinetics of tissue distribution and blood–brain barrier penetration. Int J Pharm. 2011;416:331–8.
54. Buckley A, Davidson JM, Kamerath CD, Wolt TB, Woodward SC. Sustained release of epidermal growth factor accelerates wound repair. Proc Natl Acad Sci U S A. 1985;82:7340–4.
55. Ma, J.; Wang, Q.; Fei,T.; Han, J.D.; Chen, Y.G. MCP-1 mediates TGF-beta-induced angiogenesis by stimulating vascular smooth muscle cell migration. Blood 2007, 109, 987–994.
56. Galperin A, Long TJ, Ratner BD. A Degradable, Thermo-sensitive poly(N-isopropyl acrylamide)-based scaffold with controlled porosity for tissue engineering applications. Biomacromolecules. 2010;11:2583–92.
57. Li H, Wang L, Ye L, Mao Y, Xie X, Xia C, et al. Influence of Pseudomonas aeruginosa quorum sensing signal molecule N-(3-oxododecanoyl) homoserine lactone on mast cells. Med Microbiol Immunol. 2009;198:113–21.
58. Artuc M, Hermes B, Steckelings UM, Grutzkau A, Henz BM. Mast cells and their mediators in cutaneous wound healing – active participants or innocent bystanders? Exp Dermatol. 1999;8:1–16.
59. Zhang F, Oswald T, Lin S, Cai Z, Lei M, Jones M, et al. Vascular endothelial growth factor (VEGF) expression and the effect of exogenous VEGF on survival of a random flap in the rat. Br J Plast Surg. 2003;56:653–9.
60. Tian J, Wong KKY, Ho CM, Lok CN, Yu WY, Che CM, et al. Topical delivery of silver nanoparticles promotes wound healing. Chem.Med.Chem. 2007;2:129–36.
61. Liu X, Wang Z, Wang R, Zhao F, Shi P, Jiang Y, et al. Direct comparison of the potency of human mesenchymal stem cells derived from amnion tissue, bone marrow and adipose tissue at inducing dermal fibroblast responses to cutaneous wounds. Int J Mol Med. 2013;31:407–15.
62. Yang R, Thomas GR, Bunting S. Effects of vascular endothelial growth factor on hemodynamics and cardiac performance. J Cardiovasc Pharmacol. 1996;27:838–44.
63. Guo C, Buranych A, Sarkar D, Fisher PB, Wang XY. The role of tumor-associated macrophages in tumor vascularization. Vascular Cell. 2013;5:20–32.
64. Dyken SJV, Locksley RM. Interleukin-4- and interleukin-13-mediated alternatively activated macrophages: roles in homeostasis and disease. Annu Rev Immunol. 2013;31:317–43.
65. Quentin EHL, Drugea AJ, Duffner LA, Quinn DG, Cook DN, Rollins BJ, et al. Wound healing in MIP-1$\alpha^{-/-}$ and MCP-1$^{-/-}$ mice. Am J Pathol. 2001;159:457–63.
66. Werner S, Grose R. Regulation of wound healing by growth factors and cytokines. Physiol Rev. 2003;83:835–70.
67. Casalini P, Iorio MV, Galmozzi E, Ménard S. Role of HER receptors family in development and differentiation. J Cell Physiol. 2004;200:343–50.
68. Laughner E, Taghavi P, Chiles K, Mahon PC, Semenza GL. HER2 (neu) signaling increases the rate of hypoxia-inducible factor 1α (HIF-1α) synthesis: novel mechanism for HIF-1-mediated vascular endothelial growth factor expression. Mol Cell Biol. 2001;21:995–4004.
69. Huang TH, Morrison SLA. Trimeric anti-HER2/neu ScFv and tumor necrosis factor-α fusion protein induces HER2/neu signaling and facilitates repair of injured epithelia. J Pharmacol Exp Therap. 2006;316:983–91.
70. Giordano A, Gao H, Anfossi S, Cohen E, Mego M, Lee BN, et al. Epithelial-mesenchymal transition and stem cell markers in patients with HER2-positive metastatic breast cancer. Mol Cancer Ther. 2012;11:2526–34.
71. Rao TP, Kuhl M. An updated overview on Wnt signaling pathways: a prelude for more. Circ Res. 2010;106:1798–806.